*Journal of the Geological Society, London,* Vol. **154,** 1997, pp. 935–946, 8 figs, 3 tables. Printed in Great Britain

# Geochemical and isotopic constraints on subduction polarity, magma sources, and palaeogeography of the Kohistan intra-oceanic arc, northern Pakistan Himalaya

M. ASIF KHAN[1], ROBERT J. STERN[2], ROBERT F. GRIBBLE[2] & BRIAN F. WINDLEY[3]

[1]*Centre for Excellence in Geology, Peshawar University, Peshawar, Pakistan*

[2]*Center for Lithospheric Studies, University of Texas at Dallas, Box 830688, Richardson, TX 75083-0688, USA (e-mail: rjstern@utdallas.edu)*

[3]*Department of Geology, University of Leicester, Leicester LE1 7RH, UK*

**Abstract:** Geochemical and isotopic data are presented for 18 representative samples from the intra-oceanic phase of the Kohistan arc. A restricted range of initial $^{87}Sr/^{86}Sr$ (0.7036–0.7066) and εNd (+2.8 to +7.4) along with measured $^{206}Pb/^{204}Pb$ (18.0–18.6) are consistent with formation of the arc complex in an intra-oceanic setting. The isotopic data demonstrate the involvement of enriched, DUPAL-type mantle, suggesting that the Kohistan arc formed at or south of the present equator. Subduction polarity inferred from geochemical and isotopic data indicate that the Chalt Volcanics and Kamila Amphibolites represent a forearc and backarc basin sequence, respectively. These inferences are most simply resolved with a tectonic model whereby the intra-oceanic Kohistan arc evolved over a south-dipping subduction zone, implying that Kohistan and India moved northwards on the same plate, although separated, during much of Cretaceous time. Collision of Kohistan with the Karakorum caused a new, north-dipping subduction zone to form on the south side of Kohistan, leading to collision with India in early Tertiary time.

**Keywords:** Himalayas, Pakistan, island arcs, isotopes.

The Kohistan terrane of northern Pakistan is a superb example of juvenile crust that formed by magmatic additions at an intra-oceanic convergent margin (Hamilton 1994). It is particularly important to tectonicists because its formation and accretion history constrains the Cretaceous palaeogeography of the Neotethys, and to igneous geochemists because it provides a complete and well-exposed section of primitive arc crust. Almost no isotopic data has been previously reported for the Kohistan intraoceanic arc terrane, and several important aspects about its tectonic significance remain controversial, particularly how wide was the oceanic seaway that separated it from Asia, and what was Kohistan's subduction polarity? We report here new major and trace element and isotopic compositions for igneous rocks that formed during the evolution of Kohistan as an intra-oceanic arc, and use these data to (1) confirm that Kohistan represents an intra-oceanic arc; (2) demonstrate that, prior to collision with the Karakorum terrane, the Kohistan arc faced north over a south-dipping subduction zone; and (3) infer that the Kohistan intra-oceanic arc originated near the present location of the DUPAL isotopic anomaly, at near equatorial latitudes.

## Geological setting

The Kohistan terrane is located in northern Pakistan and is bounded to the north by the Shyok (or Northern) Suture and to the south by the Indus Suture (Fig. 1). Sedimentary sequences indicate that formation of the intra-oceanic Kohistan arc began in Early Cretaceous time (Yasin Group carbonates of Aptian–Albian age; Pudsey 1986), consistent with Ar/Ar and Rb/Sr ages indicating that the bulk of the igneous infrastructure formed between 110 and 90 Ma (Schärer *et al.* 1984; Petterson & Windley 1985; Treloar *et al.* 1989). The inference that Kohistan originated as an intra-oceanic arc results from its mafic bulk composition, presence of pillowed lavas and marine sediments, low-K nature of associated felsic rocks, absence of continental crust or detritus, and separation of the inferred intra-oceanic arc of Kohistan from continental crust to the north and south by unequivocal suture zones. Kohistan and Ladakh comprise correlative parts of this Cretaceous intraoceanic arc separated by the late Cenozoic Nanga Parbat–Haramosh uplift. The intraoceanic phase of Kohistan lasted until sometime between 102 and 85 Ma, when Kohistan collided with the Karakorum (Asia) across the Shyok Suture (Treloar *et al.* 1996). From this time until collision with India about 50 Ma ago, Kohistan existed as an Andean-type margin. For a current overview of the geology of Kohistan see Treloar *et al.* (1996). This report focuses on the intra-oceanic phase of Kohistan.

The intra-oceanic arc crust of Kohistan consists of five principal units, extending from the Indus Suture in the south to the Shyok Suture in the north (Fig. 1): (1) basal ultramafic–mafic cumulates (Jijal Ultramafics); (2) Kamila Amphibolite; (3) Chilas Complex of mafic to intermediate plutonic rocks; (4) early bimodal suite of intrusive rocks (Stage 1 of Petterson & Windley 1985) and Gilgit gneisses; and (5) Chalt Volcanics (Khan *et al.* 1993). The early bimodal suite is a small part of the region shown as 'Kohistan batholith' in Fig. 1. The bulk of the Kohistan batholith formed after collision of Kohistan and Karakorum, during the Andean-margin phase of Kohistan, and is of no concern to this report. We report geochemical and isotopic data on Kamila amphibolites, Chilas Complex intrusive rocks, and Chalt Volcanics.

The Kamila Amphibolite belt is a composite mass dominated by amphibolite-facies meta-plutonic and meta-volcanic rocks. Hornblende Ar–Ar cooling ages of about

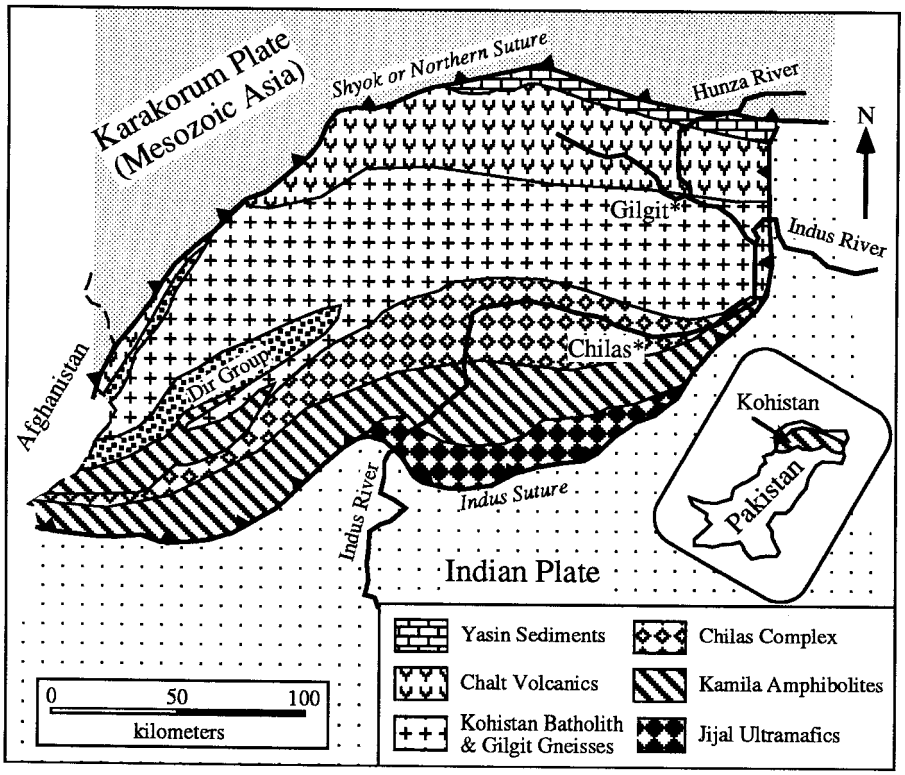


**Fig. 1.** Simplified geological map of the Kohistan terrane (modified after Coward *et al.* 1986).

80 Ma (Treloar *et al.* 1989) indicate that regional amphibolite facies conditions existed prior to this time. Two types of amphibolites are identified in the field: (1) fine- to medium-grained amphibolites, either homogeneous or banded and (2) homogeneous, medium-to coarse-grained amphibolites (Jan 1988; Treloar *et al.* 1990). The former are thought to be metamorphosed mafic to intermediate volcanics, whereas the latter are interpreted as metamorphosed gabbros and diorites. Our study was concerned with the metavolcanic amphibolites; we report no data for the second group. The Kamila metavolcanic amphibolites are subdivided into HFSE-enriched and -depleted groups, and are referred to as 'E-type' and 'D-type' metavolcanic amphibolites by Khan *et al.* (1993). E-type amphibolites have MORB-like major and trace element compositions and do not show spikes in normalized trace element patterns characteristic of subduction-related igneous rocks. In addition they show REE patterns with modest depletions in LREE. In contrast, D-type amphibolites show normalized trace element patterns consistent with the participation of a 'subduction component' (Pearce 1984). Kamila amphibolites derived from metamorphosed plutonic rocks show a very strong 'subduction component', with high Ba/Nb. Kamila metaplutonic amphibolites are compositionally very similar to gabbronorites of the Chilas Complex. Khan *et al.* (1993) concluded that all three varieties of Kamila amphibolites were derived from a mantle source that was enriched in incompatible trace elements.

The Chilas Complex is more than 300 km long and up to 40 km wide, defining the spine of the Kohistan terrane. The Chilas Complex is subdivided into 'main gabbronorites' and a 'UMA association' by Khan *et al.* (1989). Gabbronorites comprise the vast bulk of the Chilas Complex; the distinctive cumulate ultramafic, mafic, and anorthositic rocks of the UMA association formed later. Gabbronorites define a calc-alkaline suite that range from about 51 to 59% $SiO_2$, comparable to island-arc non-cumulates of Beard (1986). They show the distinctive chemical characteristics of convergent margin magmas, especially strongly positive spikes for Ba, K, and Sr, and negative Nb anomalies. They have modest LREE-enrichments ($(Ce/Yb)_n = 2–3.5$), with REE contents of about $10 \times$ chondritic abundances. The rocks cooled and equilibrated under *P–T* conditions of the pyroxene granulite facies, estimated at 750–850°C and 5–6.5 kbar (Jan & Howie 1980). In spite of the close temporal and spatial affinities of the two principal Chilas Complex components, significant differences in mineral compositions exist between gabbronorites (Olivine absent, magnetite-ilmenite, $An_{40}–An_{64}$) and UMA (Olivine abundant, Cr-spinel, $An_{83}–An_{99}$). The Chilas Complex was emplaced at *c.* 100 Ma into high levels of the deformed arc. For this report, we accept the Chilas Complex as developed during the intra-oceanic phase of Kohistan arc evolution, although Treloar *et al.* (1996) conclude that the Chilas Complex was emplaced after Kohistan collided with the Karakorum.

The Chalt Volcanics occupy a 330 km × 30 km belt along northernmost Kohistan. The upper part of these volcanics are interbedded with the Yasin sediments of Aptian–Albian age. Abundant pillowed lavas demonstrate that some if not all of these lavas erupted subaqueously. The Yasin and Chalt are strongly deformed and modestly metamorphosed, from lower greenschist facies in the west to lower amphibolite facies in the east (Petterson & Windley 1991). A significant compositional difference is observed along the strike of the belt, with a high-Mg suite encountered in the Hunza Valley (where the present suite was obtained) and a low to intermediate Mg calc-alkaline sequence found to the west. Boninite is common in the Hunza Valley section along with some tholeiitic basalts and abundant felsic lavas.

**Table 1.** *Major* and trace element and isotopic data, Kamila Amphibolites*

| | E-type | | | D-type | | |
|---|---|---|---|---|---|---|
| | A83 | A86 | A93 | A119 | A121 | A125 |
| $SiO_2$ | 51.2 | 48.0 | 48.7 | 49.5 | 50.3 | 48.7 |
| $TiO_2$ | 2.24 | 2.13 | 1.86 | 0.69 | 0.47 | 0.75 |
| $Al_2O_3$ | 14.31 | 14.44 | 14.71 | 15.90 | 16.36 | 19.11 |
| $Fe_2O_3^T$ | 14.67 | 14.08 | 13.06 | 9.08 | 8.93 | 9.15 |
| MgO | 5.11 | 6.11 | 6.90 | 11.17 | 8.18 | 6.50 |
| CaO | 9.63 | 11.64 | 11.82 | 9.83 | 12.28 | 12.01 |
| $Na_2O$ | 2.40 | 3.09 | 2.66 | 3.22 | 2.81 | 2.52 |
| $K_2O$ | 0.26 | 0.32 | 0.08 | 0.38 | 0.57 | 1.06 |
| $P_2O_5$ | 0.19 | 0.21 | 0.17 | 0.19 | 0.12 | 0.17 |
| Ni | 22 | 75 | 58 | 207 | 56 | 83 |
| Zr | 139 | 149 | 114 | 41 | 23 | 53 |
| Y | 53 | 52 | 40 | 18 | 13 | 18 |
| Nb | 4.8 | 6.2 | 4.3 | 2.6 | 1.0 | 5.0 |
| Rb | 2 | 2 | 1 | 9 | 10 | 27 |
| Sr | 150 | 137 | 169 | 233 | 268 | 257 |
| Nd† | 15.4 | 16.6 | 12.7 | 8.4 | 5.8 | 14.0 |
| Sm† | 5.3 | 5.5 | 4.2 | 2.3 | 1.74 | 3.4 |
| Pb† | 3.28 | 2.01 | 0.57 | | | 7.03 |
| K/Rb | 1080 | 1330 | 660 | 350 | 470 | 330 |
| Sr/Nd | 9.7 | 8.3 | 13.3 | 27.7 | 46.2 | 18.4 |
| $^{87}Sr/^{86}Sr$ | 0.70388 | 0.70384 | 0.70366 | 0.70417 | 0.70467 | 0.70467 |
| $^{87}Sr/^{86}Sr_i$ | 0.70381 | 0.70377 | 0.70363 | 0.70398 | 0.70449 | 0.70415 |
| $^{143}Nd/^{144}Nd$ | 0.51302 | 0.51299 | 0.51301 | 0.51284 | 0.51283 | 0.51274 |
| εNd(120) | +7.4 | +7.0 | +7.4 | +4.7 | +4.2 | +2.9 |
| $^{206}Pb/^{204}Pb$ | 17.973 | 18.128 | 18.087 | 18.073 | 18.033 | 18.462 |
| $^{207}Pb/^{204}Pb$ | 15.561 | 15.497 | 15.456 | 15.527 | 15.535 | 15.586 |
| $^{208}Pb/^{204}Pb$ | 37.951 | 38.080 | 37.979 | 38.170 | 38.039 | 38.644 |
| $\Delta^{207}Pb$‡ | 12 | 4.1 | 0.4 | 7.7 | 8.9 | 9.4 |
| $\Delta^{208}Pb$‡ | 59 | 54 | 48 | 69 | 61 | 70 |

*Major element totals normalized to 100%, anhydrous.
†Analysis by isotope dilution.
$^{87}Sr/^{86}Sr_i$, εNd(120) calculated using $t = 120$ Ma and Rb/Sr, Sm/Nd listed above.
‡Deviations from Northern Hemisphere Reference Line (Hart 1984).

## Analytical techniques

Major- and trace-element analyses presented in Tables 1, 2, and 3 were obtained using standard XRF spectrometry techniques. The samples of Kamila Amphibolite and the Chilas Complex were analysed at the University of Oklahoma, using a Rigaku XRF, while those from the Chalt Volcanics were analysed at the University of Leicester, using Philips PW 1450 automatic XRF. Similar analytical techniques and standards were used at the two laboratories. Major elements were determined from glass fusion beads (made using a lithium tetraborate/lithium metaborate flux; rock:flux ratio 1:5) analysed by using a Rh anode X-ray tube. Trace element concentrations were determined on pressed-powder pellets made using an organic binder (Moviol). Ni, Zr, Nb, Rb, Sr, Y determinations were made using a Rh anode X-ray tube with mass absorption corrections applied using the intensities of the Rh Kα Compton scatter peak (Harvey & Atkins 1982). Determinations of Cr and Ba used a W anode X-ray tube with mass absorption corrections applied using the intensities of the W Lα Rayleigh scatter peak and Fe Kα to cross the Fe-absorption edge after the technique of Nesbitt *et al.* (1976). Detections limits (2 sigma) are approximately 1 ppm for Cr, Rb, Sr, Zr, Nb and Y, and 2 ppm for Ni, Cr and Ba.

Concentrations of Nd, Sm, and Pb were determined by isotope dilution at UTD. Standard isotope dilution and cation exchange techniques were used to separate Sr, and LREE (Nd & Sm). A procedure modified after Richard *et al.* (1976) was used to separate Nd from Sm for isotope composition runs. The Pb separation procedure is reported in Manton (1988), with an initial anionic column separation. Total processing blanks were: <140 pg Pb; <700 pg Nd; and <1 ng Sr. Isotopic compositions were determined with a Finnigan MAT 261 multi-collector thermal ionization mass spectrometer; Nd was analysed in the dynamic multicollection mode, whereas Sr and Pb were analysed in the static multicollection mode. Sr isotopic compositions were fractionation-corrected to $^{86}Sr/^{88}Sr = 0.1194$ and adjusted relative to E&A $SrCO_3$ $^{87}Sr/^{86}Sr = 0.70800$. Nd isotopic compositions were fractionation-corrected to $^{146}Nd/^{144}Nd = 0.7219$ and εNd was calculated using the εNd values of Pier *et al.* (1989) for BCR-1 and UCSD standards. The standard values with reproducibility during the year in which isotopic analyses were carried out ( ± 1 standard deviation, with digits corresponding to the last decimal places reported) were: E&A $SrCO_3$ $^{87}Sr/^{86}Sr = 0.708020$ (35; $n = 32$), UCSD $^{143}Nd/^{144}Nd = 0.511848$ (14; $n = 26$), and BCR-1 $^{143}Nd/^{144}Nd = 0.512620$ (8; $n = 8$); NBS 981 (with 0.15% per amu Pb fractionation correction) $^{206}Pb/^{204}Pb = 16.943$ (13), $^{207}Pb/^{204}Pb = 15.495$ (17), $^{208}Pb/^{204}Pb = 36.736$ (50) for 16 analyses.

Sr and Nd isotopic compositions listed in Tables 1 to 3 are reported both as measured following fractionation correction ($^{143}Nd/^{144}Nd$) and, in the case of Sr, adjustment to a value of 0.70800 for E&A $SrCO_3$ $^{87}Sr/^{86}Sr$, as well as initial isotopic compositions, corrected for 120 Ma of radiogenic growth using values of $^{147}Sm/^{144}Nd$ and $^{87}Rb/^{86}Sr$ from element abundances listed in Tables 1 to 3. Initial isotopic compositions are reported either as $^{87}Sr/^{86}Sr_i$ or as $\varepsilon Nd_{(120)}$. Pb isotopic compositions are recalculated using the Δ notation of Hart (1988), which specifies the extent to which $^{207}Pb/^{204}Pb$ and $^{208}Pb/^{204}Pb$ are distinct from a reference line defined by oceanic basalts from the northern hemisphere. This notation is used because it is an effective way to identify igneous rocks derived from certain mantle reservoirs such as the DUPAL source. Because U and Th concentrations have not been determined, the Pb isotopic compositions could not be

**Table 2.** *Major* and trace element and isotopic data, Chilas Complex*

| | UMA | | Main gabbronorites | |
|---|---|---|---|---|
| | IK 1007 | IK 1009 | IK 1012 | IK 1017 |
| $SiO_2$ | 45.9 | 43.0 | 52.5 | 58.4 |
| $TiO_2$ | 0.07 | 0.22 | 1.24 | 0.84 |
| $Al_2O_3$ | 24.09 | 3.77 | 18.28 | 17.80 |
| $Fe_2O_3^T$ | 4.67 | 18.95 | 9.45 | 7.93 |
| MnO | 0.07 | 0.24 | 0.12 | 0.12 |
| MgO | 9.45 | 30.42 | 5.31 | 3.91 |
| CaO | 15.41 | 3.37 | 9.44 | 7.39 |
| $Na_2O$ | 0.35 | 0.00 | 2.74 | 3.04 |
| $K_2O$ | 0.01 | 0.00 | 0.66 | 0.35 |
| $P_2O_5$ | 0.01 | 0.02 | 0.25 | 0.18 |
| Ni | 169 | 819 | 33 | 18 |
| Cr | 397 | 1208 | 56 | 36 |
| Zr | 5 | 5 | 71 | 133 |
| Nb | — | — | 3.7 | 4 |
| Rb | <1 | <1 | 7 | <1 |
| Sr | 427 | 64 | 403 | 446 |
| Ba | 18 | 19 | 211 | 246 |
| Nd† | 0.81 | 0.73 | 13.6 | 13.0 |
| Sm† | 0.25 | 0.25 | 3.56 | 3.29 |
| Pb† | — | — | — | — |
| K/Rb | — | — | 780 | — |
| Sr/Nd | 527 | 87.7 | 29.6 | 34.3 |
| $^{87}Sr/^{86}Sr$ | 0.70405 | 0.70404 | 0.70423 | 0.70412 |
| $^{87}Sr/^{86}Sr_i$ | 0.70404 | 0.70396 | 0.70414 | 0.70411 |
| $^{143}Nd/^{144}Nd$ | 0.51280 | 0.51284 | 0.51274 | 0.51274 |
| εNd(120) | +3.5 | +4.0 | +2.8 | +2.9 |
| $^{206}Pb/^{204}Pb$ | 18.526 | 18.574 | 18.554 | 18.526 |
| $^{207}Pb/^{204}Pb$ | 15.640 | 15.623 | 15.627 | 15.624 |
| $^{208}Pb/^{204}Pb$ | 38.762 | 38.671 | 38.783 | 38.746 |
| $\Delta^{207}Pb$‡ | 14 | 12 | 13 | 12 |
| $\Delta^{208}Pb$‡ | 74 | 59 | 72 | 72 |

*Major element totals normalized to 100%, anhydrous.
†Analysis by isotope dilution.
$^{87}Sr/^{86}Sr_i$, εNd(120) calculated using $t = 120$ Ma and Rb/Sr, Sm/Nd listed above.
‡Deviations from Northern Hemisphere Reference Line (Hart 1984).

recalculated as initial ratios. However, the isotopic composition of Pb in the samples may still be a useful isotopic fingerprint for the following reasons: (1) relatively little isotopic growth is expected to have occurred (see modelled growth in Fig. 4); and (2) relatively modest fractionation of U, Th, and Pb is expected during generation of mafic melts from the mantle (Zartman & Doe 1981). The Pb isotopic characteristics of Kohistan samples are similar to the DUPAL mantle reservoir, and this is not likely to be a result of post-eruption radiogenic growth.

## Results

The investigated Kamila samples are all mafic, with a restricted range in silica (48–52%) but with a much wider range in incompatible elements such as K (Fig. 2). The subdivision of the Kamila metavolcanic amphibolites into E-type (relatively high Ti and other HFSE such as Zr, Y, and Nd; relatively low $K_2O$, Rb, and Sr) and D-type is supported by trace element ratios (E-type has high K/Rb = 660–1330 and low Sr/Nd = 8–13 characteristic of MORB and ocean island basalt (OIB), whereas D-type has low K/Rb = 330–470 and high Sr/Nd = 18–46, similar to that of modern convergent margin volcanic suites). All of these features are consistent with E-type Kamila metavolcanic amphibolites having a MORB-like basaltic precursor, whereas D-type Kamila metavolcanic amphibolites have clear characteristics of supra-subduction zone igneous rocks. We will show that Kamila D-type metavolcanics are similar in many respects to the rocks of the Chilas plutonic complex.

The isotopic data also distinguish between the two types of Kamila metavolcanic amphibolites. E-type samples have more radiogenic Nd ($\varepsilon Nd_{120\ Ma} = +7.0$ to $+7.4$) and less radiogenic initial Sr ($^{87}Sr/^{86}Sr = 0.7036$–$0.7039$) than the three D-type samples ($\varepsilon Nd_{120\ Ma} = +2.9$ to $+4.7$; $^{87}Sr/^{86}Sr = 0.7041$–$0.7047$). E-type and D-type amphibolites plot in distinct locations in a plot of Sr-Nd isotopes (Fig. 3). The Pb isotopic compositions of E- and D-type metavolcanics are similar (Fig. 4). Kamila E-type amphibolites have the most radiogenic Nd and least radiogenic Sr and $^{206}Pb/^{204}Pb$ of all the Kohistan samples that we have analysed. Kamila D-type metavolcanic amphibolites are similar to Chilas samples in having relatively low $\varepsilon Nd_{120\ Ma}$ and high $^{87}Sr/^{86}Sr$, although only one of the D-type Kamila samples (A125) has a similar Pb isotopic composition. A puzzling feature is that Kamila amphibolites have homogeneous and relatively non-radiogenic $^{206}Pb/^{204}Pb$ and $^{208}Pb/^{204}Pb$, but have variable $^{207}Pb/^{204}Pb$.

Of the four Chilas samples that were analysed, two are from the Main Gabbronorites and two are from the UMA. UMA samples are cumulates, so it is difficult to infer much regarding their petrotectonic setting from their chemical compositions. The gabbronorite samples on the other hand may approximate melt compositions; they are mafic to intermediate and belong to a low-K to moderate K suite. Gabbronorites have high K/Rb and Sr/Nd; we can infer from their Sm and Nd abundances that these were moderately enriched in LREE. The isotopic composition of the four Chilas samples is very homogeneous, with $^{87}Sr/^{86}Sr_i = 0.70396$–$0.70414$, $\varepsilon Nd_{(120)} = +2.8$ to $+4.0$, and very homogenous Pb. Along with one sample of D-type Kamila amphibolite (A125), the Chilas complex defines the relatively 'enriched' endmember of the Kohistan intra-oceanic arc terrane. The Chilas Complex samples and some D-type Kamila amphibolites extend towards an EMI isotopic reservoir in Sr–Nd isotopic space, but extend towards EMII in Pb isotopic space.

The Chalt Volcanics define a compositionally heterogeneous group. They include low-K and medium-K rocks of basaltic, boninitic, and rhyodacitic composition (Fig. 2). The suite is characterized by very low $TiO_2$ and Zr contents (<0.45% and <80 ppm, respectively). Chalt boninites and low-Ti basalts may contain very high contents of MgO (up to 12.5%), Ni (up to 400 ppm), and Cr (up to 1500 ppm). Boninitic samples (PL28, N138, N161, and IK580) have 10 to 12.5% CaO, and must therefore be classified as 'High Ca boninites' according to Crawford *et al.* (1989). Basalts and boninites have very low abundances of Sr (<100 ppm), Ba (<40 ppm), and Nd (<8 ppm).

Samples of the Chalt Volcanics that we analysed have homogeneous isotopic compositions of Nd ($\varepsilon Nd(120\ Ma) = +6.3$ to $+7.3$) and Pb ($^{206}Pb/^{204}Pb = 18.1$–$18.4$ $\Delta^{208}Pb = 44$–$58$; $\Delta^{207}Pb = 5$–$10$). The 8 samples of Chalt boninite, basalt, and rhyodacite fall between Kamila and Chilas suites on plots of Pb isotopic compositions (Fig. 4). The Chalt Volcanics define a much larger range on a plot of Sr v. Nd isotopic compositions (Fig. 3), reflecting the larger range in $^{87}Sr/^{86}Sr_i$ (0.7040–0.7055). The Chalt Volcanics are metamorphosed submarine lavas, probably reflecting partial re-equilibration accompanying submarine hydrothermal metamorphism. Such

**Table 3.** *Major* and trace element and isotopic data, Chalt Volanics*

| | PL28 | PL29 | N115 | N116 | N138 | N139 | N161 | IK580 |
|---|---|---|---|---|---|---|---|---|
| $SiO_2$ | 53.5 | 64.6 | 76.0 | 49.7 | 60.1 | 72.1 | 52.1 | 56.5 |
| $TiO_2$ | 0.21 | 0.42 | 0.28 | 0.30 | 0.23 | 0.31 | 0.21 | 0.27 |
| $Al_2O_3$ | 12.25 | 17.62 | 12.52 | 13.46 | 11.79 | 12.91 | 9.44 | 12.38 |
| $Fe_2O_3{}^T$ | 9.62 | 5.32 | 2.94 | 14.61 | 7.94 | 4.92 | 8.87 | 8.17 |
| MnO | 0.19 | 0.09 | 0.05 | 0.22 | 0.18 | 0.09 | 0.18 | 0.13 |
| MgO | 11.37 | 1.75 | 0.86 | 8.52 | 8.75 | 1.24 | 15.05 | 9.74 |
| CaO | 10.34 | 3.71 | 1.91 | 9.80 | 10.11 | 3.14 | 12.53 | 10.06 |
| $Na_2O$ | 2.38 | 4.40 | 3.40 | 2.63 | 0.68 | 4.59 | 1.29 | 2.56 |
| $K_2O$ | 0.16 | 2.03 | 1.97 | 0.72 | 0.20 | 0.64 | 0.29 | 0.13 |
| $P_2O_5$ | 0.03 | 0.11 | 0.07 | 0.07 | 0.04 | 0.07 | 0.04 | 0.04 |
| Ni | 191 | 3.7 | 3.4 | 39 | 105 | 3.3 | 386 | 128 |
| Cr | 936 | 7.8 | 18 | 109 | 356 | 13 | 1521 | 627 |
| Zr | 22 | 77 | 56 | 26 | 24 | 45 | 19 | 23 |
| Y | 9.6 | 23 | 18 | 13 | 7.7 | 13 | 7.6 | 8.3 |
| Nb | 1.2 | 1.8 | 1.4 | — | 1.0 | 0.9 | — | — |
| Rb | 3.3 | 43 | 36† | 15 | 5.4 | 17 | 3.4 | 0.4 |
| Sr | 71 | 211 | 67† | 114 | 51 | 845 | 48 | 91 |
| Ba | 17 | 143 | 167 | 36 | 30 | 92 | 14 | 20 |
| Nd† | 2.13 | 6.9 | 5.3 | 7.7 | 1.36 | 3.18 | 1.25 | 1.72 |
| Sm† | 0.77 | 2.27 | 1.73 | 2.48 | 0.50 | 1.08 | 0.48 | 0.60 |
| Pb† | 1.21 | 5.4 | 1.19 | 5.5 | 1.53 | 3.6 | — | — |
| K/Rb | 400 | 390 | 450 | 400 | 310 | 310 | 710 | 2700 |
| Sr/Nd | 33.3 | 30.6 | 12.6 | 14.8 | 37.5 | 266 | 38.4 | 52.9 |
| $^{87}Sr/^{86}Sr$ | 0.70516 | 0.70544 | 0.70676 | 0.70520 | 0.70525 | 0.70493 | 0.70561 | 0.70549 |
| $^{87}Sr/^{86}Sr^i$ | 0.70493 | 0.70445 | 0.70408 | 0.70457 | 0.70455 | 0.70483 | 0.70526 | 0.70547 |
| $^{143}Nd/^{144}Nd$ | 0.51301 | 0.51301 | 0.51299 | 0.51295 | 0.51297 | 0.51297 | 0.51300 | 0.51299 |
| εNd(120) | +7.0 | +7.3 | +7.1 | +6.3 | +6.3 | +6.5 | +6.8 | +6.9 |
| $^{206}Pb/^{204}Pb$ | 18.187 | 18.226 | 18.345 | 18.243 | 18.283 | 18.299 | 18.168 | 18.113 |
| $^{207}Pb/^{204}Pb$ | 15.518 | 15.536 | 15.552 | 15.540 | 15.569 | 15.535 | 15.524 | 15.520 |
| $^{208}Pb/^{204}Pb$ | 38.113 | 38.199 | 38.340 | 38.224 | 38.315 | 38.187 | 38.124 | 38.103 |
| $\Delta^{207}Pb$‡ | 5.6 | 6.9 | 7.2 | 7.1 | 9.6 | 6.0 | 6.4 | 6.6 |
| $\Delta^{208}Pb$‡ | 50 | 54 | 53 | 54 | 58 | 44 | 53 | 58 |

*Major element totals normalized to 100%, anhydrous.
†Analysis by isotope dilution.
$^{87}Sr/^{86}Sr_i$, εNd(120) calculated using $t = 120$ Ma and Rb/Sr, Sm/Nd listed above.
‡Deviations from Northern Hemisphere Reference Line (Hart 1984).

metamorphism greatly affects Sr, but not Nd or Pb isotopic compositions. If so, the Chalt before being metamorphosed may have had as restricted a range of Sr isotopic compositions as it now has Nd and Pb isotopic compositions. The petrologic diversity of the Chalt Volcanics can be explained by a fractional crystallization process from a parental magma similar to the Chalt boninites or basalts. Nd and Pb isotopic homogeneity for the large range of $SiO_2$ contents in Chalt Volcanics supports this model, although this requires that the range in Sr isotopic composition reflects alteration. Alternatively, the isotopic data are consistent with a model of anatexis whereby Chalt boninites or basalts were melted to generate felsic lavas. It is also noteworthy that the Sr and Nd isotopic composition of the 102 ± 12 Ma Matum Das tonalite (Petterson & Windley 1985), which crops out along the Hunza River in the belt of Chalt Volcanics, has Sr and Nd isotopic compositions that indicate close petrogenetic affinities with the Chalt (Fig. 3; Petterson *et al.* 1993).

The range of $^{87}Sr/^{86}Sr_i$ for igneous rocks of the intra-oceanic Kohistan arc (0.7036–0.7056; mean = 0.7043) is similar to that for initial ratios for correlative units from Ladakh, including the Dras Volcanics (*c.* 0.7035), Kargil mafic cumulates (0.704–0.7053; Dietrich *et al.* 1983), and Ladakh intrusives (0.7034–0.7048; Honegger *et al.* 1982).

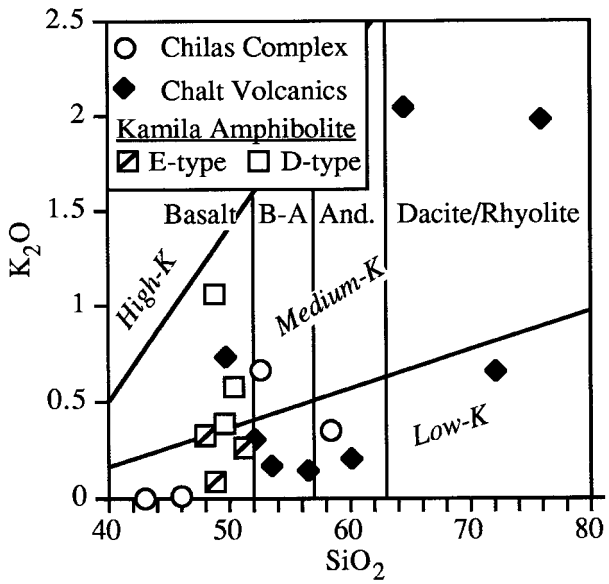


**Fig. 2.** Potassium–silica diagram for Kohistan samples. Field boundaries are from LeMaitre (1989). B-A, basaltic andesite; And, andesite.

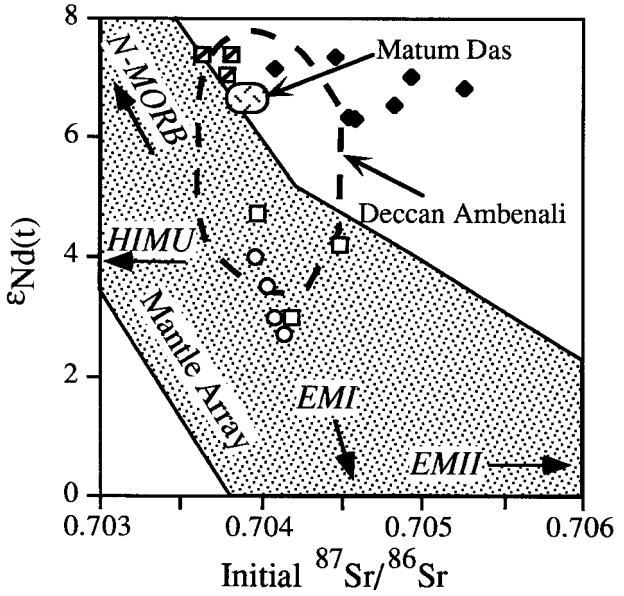


**Fig. 3.** Sr–Nd isotopic compositions of Kohistan samples. Symbols for Chalt Volcanics, Chilas Complex, and Kamila E-type and D-type amphibolites are the same as shown in Fig. 2. Isotopic composition of 102 Ma Matum Das tonalite is from Petterson *et al.* (1993). Approximate location of modern mantle array is shown for sake of comparison, along with vectors pointing towards 4 mantle reservoirs (N-MORB, HIMU, EMI, and EMII; Hart 1988). Isotopic composition of Ambenalli basalts of the Deccan Traps, India, is from Lightfoot *et al.* (1990).

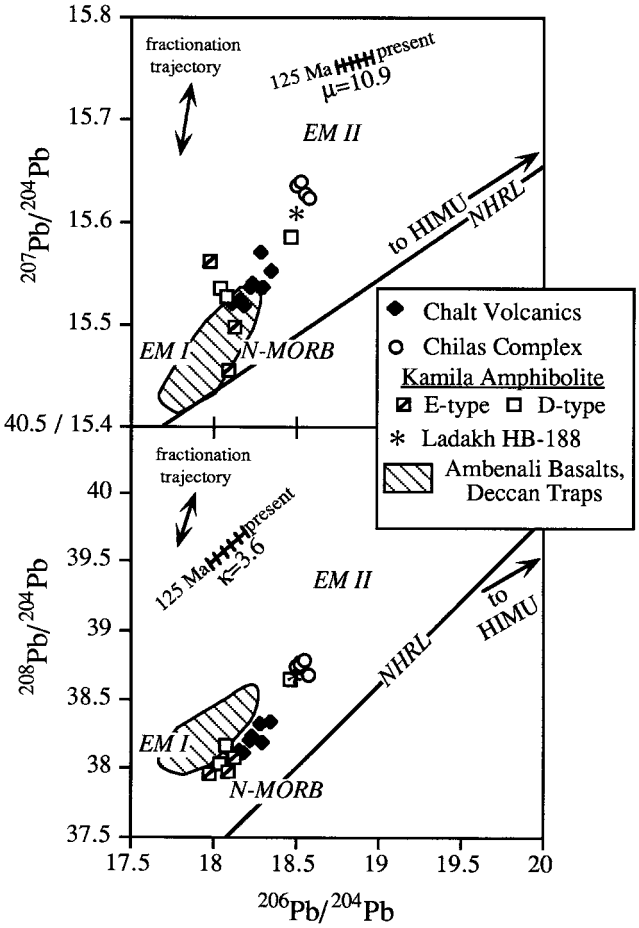


**Fig. 4.** Pb isotopic compositions of Kohistan igneous rocks. Line labelled 'NHRL' is the northern hemisphere reference line of Hart (1984). Approximate positions of model mantle reservoirs EMI, EMII, and N-MORB are shown; HIMU lies off the diagram to the right (Hart 1988). Asterisk denotes isotopic composition of Pb in K-feldspar from a 101 ± 2 Ma granodiorite from Ladakh (Schärer *et al.* 1984). Isotopic composition of Ambenali basalts, Deccan Traps, India, is from Lightfoot *et al.* (1990). Also shown are trajectories of isotopic composition corrected for radiogenic growth back to 125 Ma (25 million year steps), assuming μ ($^{238}U/^{204}Pb$) = 10.9 and κ ($^{232}Th/^{238}U$) = 3.6. This is intended to illustrate the magnitude and the general direction of isotopic changes that may have occurred in these samples since these lavas were erupted in the Cretaceous. Also shown are vectors appropriate for fractionation trajectories due to thermal fractionation during analysis; the length of the vector corresponds to ± 0.15%/amu.

## Discussion

The data presented here allow us to address three questions about the Kohistan intra-oceanic arc system. These are: (1) polarity of the intra-oceanic Kohistan arc; (2) nature of the source region of Kohistan arc magmas; (3) palaeogeographic setting of the Kohistan intra-oceanic arc. These items are discussed further below.

### *Polarity of the intra-oceanic Kohistan arc*

The intra-oceanic Kohistan–Ladakh arc formed over a subduction zone which dipped beneath it either to the south or to the north. From the time it was first recognized as an intra-oceanic arc complex (Tahirkheli *et al.* 1979), investigators have preferred the interpretation that the dip was to the north (Pudsey 1986; Petterson & Windley 1991; Robertson & Degnan 1994). We are not convinced by the evidence for a northerly dip direction for the Kohistan subduction zone prior to collision with the Karakorum. Regardless of the orientation of the subduction zone beneath Kohistan, another north-dipping subduction zone beneath Karakorum is required to generate *c.* 95 Ma granodioritic rocks of the Karakorum batholith (Le Fort *et al.* 1983). Collision between Kohistan and Karakorum to form the Shyok Suture is constrained to have occurred sometime in the early Late Cretaceous, 85–102 Ma ago (Treloar *et al.* 1989). Pudsey (1986) argued that this suture represented a collapsed back-arc basin, in part to accommodate the lack of evidence in the suture melange for subduction of a large oceanic tract.

Our understanding of the distribution of igneous rocks and their trace element and isotopic compositions in Kohistan presents another perspective for constraining subduction polarity of the intra-oceanic Kohistan arc. We conclude that the chemical and isotopic composition of Kohistan igneous rocks, particularly the Chalt and Kamila volcanic sequences, formed over a *south*-dipping subduction zone. We appreciate that our interpretation is not exclusive; for example, Treloar *et al.* (1996) infer that the Kamila provides substrate to Chalt cover. However, we find that the geochemical and isotopic data are more consistent with Kohistan sequences reflecting changes across an approximately contemporaneous arc system. There are two lines of evidence to support this. (1) The Chalt Volcanics (especially their boninitic component) are interpreted to have formed in a forearc setting (Petterson & Windley 1991). There are several models for why boninites

form in forearcs, including subduction initiation (Stern & Bloomer 1992; Bloomer *et al.* 1995), spreading-centre subduction (Crawford *et al.* 1989; Pearce *et al.* 1992), and interaction of the elevated thermal regime associated with a back-arc basin spreading center superimposed on the high water flux of a forearc (Falloon & Crawford 1991). Discussion continues regarding which of these models is most appropriate, but the consensus that boninites form in fore-arc settings remains. The interbedded submarine boninites, low-Ti tholeiites, and felsic rocks of the Chalt Volcanics are reminiscent of the Izu–Bonin–Mariana forearc, as is the rapid transition from volcanism to carbonate-dominated pelagic and hemipelagic sedimentation represented by the Chalt-Yasin succession (Bloomer *et al.* 1995). (2) The MORB-like affinities of Kamila E-type metavolcanic amphibolites and their intercalation with D-type amphibolites which have a strong subduction component is most consistent with the interpretation that these formed in a back-arc basin. MORB-like magmas are only found at convergent margins in a back-arc basin setting, and sequences containing alternating or interfingering MORB- and arc-tholeiites are characteristic of modern back-arc basins such as the Mariana Trough and Lau Basin (Wood *et al.* 1981; Hawkins 1995; Gribble *et al.* 1996).

The inference that the 'subduction component' becomes less important from the Chalt Volcanics in the north to the Kamila Amphibolites in the south is also supported by an overall increase in the incompatible HFS elements Ti and Zr in the same direction. Abundances of HFS elements in an intra-oceanic convergent margin increase from the forearc to the back-arc, which reflects an overall decrease in the degree of melting or degree of source region depletion that gives a clear facing direction for the arc (Taylor *et al.* 1992). The HFSE evidence for Kohistan is very clear; considering only rocks with 48–59% $SiO_2$, the Chalt Volcanics contain $\leq$0.3% $TiO_2$ and <30 ppm Zr; Chilas Complex samples contain 0.84 and 1.24% $TiO_2$ and 71–133 ppm Zr; Kamila samples contain as much as 2.25% $TiO_2$ and 149 ppm Zr. These relationships are graphically presented in Fig. 5, by which result the intra-oceanic Kohistan arc faced northwards above a S-dipping subduction zone.

The tectonic model that we prefer is shown in Fig. 6. Figure 6a shows the intra-oceanic phase and features an ocean basin (Neotethys) between Karakorum and Kohistan. This ocean closed as a result of two subduction zones, one dipping north beneath Karakorum and the other dipping south beneath Kohistan. This tectonic situation has a modern analogue in the Molucca Sea, south of the Philippines. The Molucca Sea is closing as a result of west-dipping subduction beneath the Sangihe Arc to the west and east-dipping subduction beneath the Halmahera Arc to the east (Hamilton 1978; Moore *et al.* 1981).

There is no evidence for a hiatus in India's northward motion during the Late Cretaceous, and continuous northward motion requires a new subduction zone to form immediately after Kohistan and Karakorum collided. This new subduction zone dipped north on the south side of Kohistan. This reversal of subduction polarity beneath Kohistan during the Late Cretaceous is analogous to the situation inferred for the Solomon Arc during the Late Tertiary (Cooper & Taylor 1985). Thickened crust of the Ontong Java Plateau arrived at the Vitiaz Trench on the north side of the Solomon Arc during the Miocene. This stopped south-dipping subduction and led to the formation of a new, north-dipping subduction zone southwest of the Solomons.

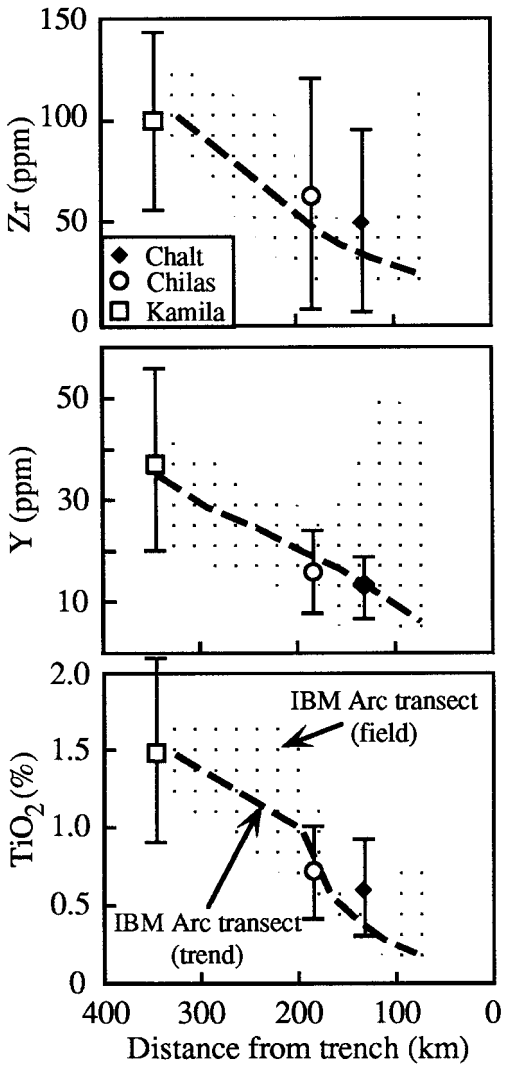


**Fig. 5.** Abundances of high field strength elements Zr, Y, and Ti for Kohistan intraoceanic phase igneous rocks, compared with data for transects across the Izu–Bonin–Mariana (IBM) intra-oceanic arc system, reported by Taylor *et al.* (1992). Stippled field encompasses all IBM data for samples, filtered for 3.5%<MgO<15%; dashed line is our estimate of the 'best fit' trend of the data. IBM Arc system data indicate increasing HFSE concentrations with distance from the trench. Data for Kohistan samples includes mean $\pm$ 1 standard deviation. Positions of Chalt, Chilas, and Kamila are shown to make the point that Kohistan HFSE data are most consistent with the sequence of units having the following order of increasing distance from the trench: Chalt, Chilas, and Kamila. This is consistent with a model for the formation of the Kohistan intra-oceanic arc system over a south-dipping subduction zone. Kohistan data sources follow: Chalt ($n$=41), Petterson & Windley (1985, 1991), Luff & Windley (unpublished); Chilas ($n$=40), Khan *et al.* (1989); Khan (unpublished); Kamila ($n$=37), Khan (unpublished).

Our model satisfies all tectonic constraints, including: (1) India began moving north during the magnetic quiet zone, at approximately 120 Ma, and continued to move rapidly north until collision with Asia about 50 Ma ago (Patriat & Achache 1984). The northward movement of India reflects the development of subduction zones to the north at about 120 Ma (Scotese *et al.* 1988). (2) North-dipping subduction is required

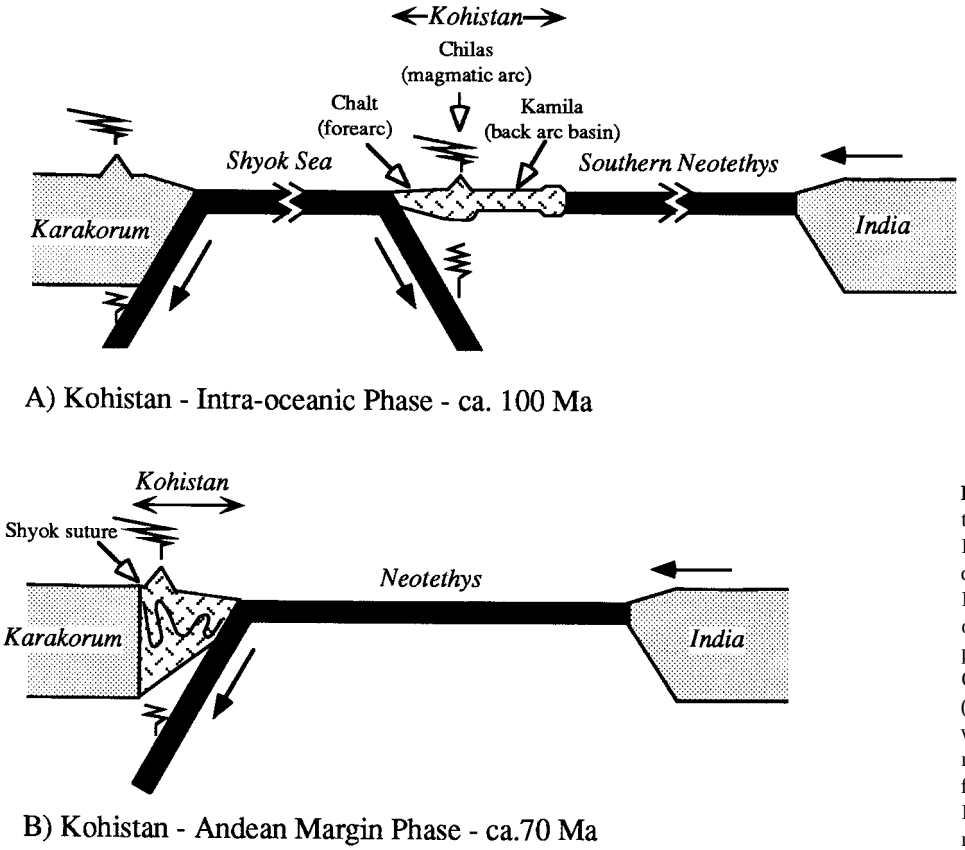


**Fig. 6.** Tectonic model for evolution of the Kohistan arc. (**a**) Intraoceanic phase. India drifts northwards (left) due to closing of an ocean basin between Karakorum and Kohistan. Kohistan is on the same plate as India. Note positions of Chalt Volcanics, Chilas Complex, and Kamila Amphibolites. (**b**) Andean phase. Kohistan has collided with Karakorum and a new, northward-dipping subduction zone has formed on the south side of accreted Kohistan. India continues to move north.

beneath Karakorum to generate the Karakorum batholith (Searle 1991). (3) Following the formation of the Shyok suture, the subduction zone associated with the northward motion of India dipped north on the south side of accreted Kohistan. This explanation is also consistent with the presence of S-dipping structures in northern Kohistan (Coward *et al.* 1982), which may have formed in association with a S-dipping subduction zone.

### *Nature of the source region of Kohistan intra-oceanic arc magmas*

One of the important controversies surrounding convergent margin magma-genesis concerns the relative contributions provided by mantle as opposed to subducted crust and sediments. Understanding this chemical budget is important not only for understanding arc magma-genesis, but also for understanding a wide range of other first-order questions about the earth, including whether or not the Earth's mantle and crust are still differentiating, whether the continents are growing or shrinking, and how the sources of hot-spot mantle formed. It is widely acknowledged that a hydrous subduction zone environment may be responsible for fractionating elements that are not fractionated in anhydrous magmagenetic environments such as hot spots or mid-ocean ridges. The most spectacular of these incompatible element fractionations in arcs is the relatively high abundance of fluid-mobile alkali metals and alkaline earths (K, Rb, Ba, Sr) relative to the abundance of less mobile high field strength elements (e.g., Ti, Zr, Y, Nb, Ta). Having acknowledged these fractionations and the fact that some elements are clearly derived from subducted components such as $^{10}$Be (Morris *et al.* 1990), the question remains as to the relative importance of contributions of other incompatible elements that are extracted from the mantle compared to those that are recycled from subducted crust and sediments.

We argue that the distinctive isotopic signature of Indian Ocean mantle is readily recognized in the composition of Kohistan igneous rocks, and that this signature overwhelms any signature from subducted sediment. Hart (1984) recognized a zone of enriched mantle underlying equatorial oceanic regions which he called DUPAL. DUPAL mantle generates lavas with distinctive isotopic characteristics, including relatively low εNd and $^{206}$Pb/$^{204}$Pb, and relatively high $^{87}$Sr/$^{86}$Sr and Δ8/4. Regions underlain by DUPAL mantle are presently far to the south of Kohistan, but DUPAL isotopic characteristics are readily identified in all igneous rocks from the intraoceanic phase of the Kohistan arc (Fig. 7).

Another perspective is gained from comparison of Kohistan igneous rocks with Deccan traps. The Deccan Traps are flood basalts that erupted about 65 Ma when India passed over the Reunion hotspot. Most of the Deccan basalts have been significantly contaminated by continental lithosphere, but the Ambenali unit in the upper part of the sequence is thought to manifest predominantly asthenospheric isotopic compositions (Lightfoot & Hawkesworth 1988; Peng & Mahoney 1995). The Ambenali basalts formed about 3500 km south of their present position and thus represent the composition of the asthenosphere beneath the subequatorial Indian Ocean basin at the end of Cretaceous time. They show DUPAL isotopic characteristics, especially high Δ8/4, and constitute an appropriate data set that can be used to examine the potential mantle controls on the isotopic composition of Kohistan igneous rocks.

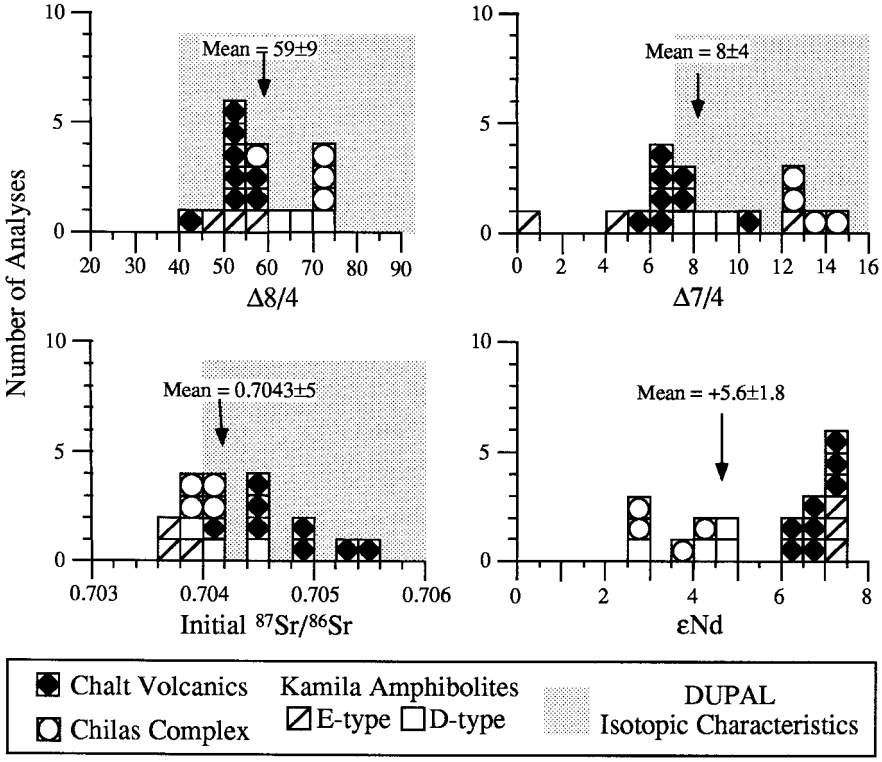


**Fig. 7.** Histogram of initial isotopic composition of Sr and Nd and measured Pb istopic compositions reported using Δ notation of Hart (1984). Means ( ± 1 std. dev.) are for the entire Kohistan suite. Stippled field labelled 'DUPAL Isotopic Characteristics' are taken from Hart (1984) for Sr and Pb; DUPAL Nd isotopic characteristics are not given by Hart (1984).

Six samples of Ambenali basalts analysed by Lightfoot *et al.* (1990) have εNd of +4.3 to +7.5 and $^{87}Sr/^{86}Sr$ of 0.7039–0.7046, very similar to the range of Kohistan igneous rocks (εNd = +2.8 to +7.4 and $^{87}Sr/^{86}Sr$ = 0.7036–0.7055). The similarity of the Sr–Nd isotopic systematics of Kohistan and Ambenali igneous rocks is shown in Fig. 3. Differences between the Sr and Nd isotopic systematics of Kohistan igneous rocks and Ambenali basalts consist of extension of the Kohistan suite to slightly lower εNd that nevertheless lie within the mantle array, and the higher $^{87}Sr/^{86}Sr$ of the Chalt Volcanics. The Pb isotopic compositions of Kohistan igneous rocks are also similar to those of Ambenali basalts, as shown on Fig. 4. The Ambenali basalts have a somewhat lower range of $^{206}Pb/^{204}Pb$ (17.7–18.3) than Kohistan rocks (17.9–18.6), but are similar in lying above the northern hemisphere reference line (NHRL) in similarly distinctive fashions. On a plot of $^{207}Pb/^{204}Pb$ v. $^{206}Pb/^{204}Pb$ (Fig. 4), both define a trend that obliquely intersects NHRL at $^{206}Pb/^{204}Pb \approx 17.6$ and extends towards the EMII reservoir. On a plot of $^{208}Pb/^{204}Pb$ v. $^{206}Pb/^{204}Pb$, both define a trend which lies above and parallel to NHRL. The Pb isotopic characteristics for both Kohistan and Ambenali are consistent with mixing between mantle reservoirs EMI and EMII. Intriguingly, evidence of such mixing cannot be inferred from Sr–Nd systematics (Fig. 3).

### *Palaeogeographic setting of the Kohistan intra-oceanic arc*

Our inferences regarding polarity of the intra-oceanic Kohistan arc and its formation in an oceanic realm dominated by DUPAL mantle sources lead us to propose a palaeogeographic model for Early Cretaceous time (Fig. 8). It shows Kohistan lying within the DUPAL region, about 3000 km south of the Karakorum. The Shyok Sea, that part of Neotethys north of Kohistan, lies between Kohistan and Karakorum. India and Karakorum move northwards together until Kohistan collides with Karakorum, when a new, north-dipping subduction zone is constructed on the south flank of Kohistan. The development of this new subduction zone may be manifested by the first stages in the development of the Oman subduction zone (obduction of the Semail ophiolite), about 90–95 Ma (Lippard *et al.* 1986).

This model is subject to a number of uncertainties which affect the size of the seaway that lay between Kohistan and southern Asia. First of all, the location of the southern margin of Asia at this time is controversial. For example, we present the configuration of Scotese *et al.* (1988) which places it about 15°N, but Searle (1991) places it closer to 10°N. Secondly, the location of Kohistan is not highly constrained. It must lie between India and Asia, and we infer from the isotopic data that it lay in the DUPAL realm, but where precisely? We have also assumed that the surface projection and location of the DUPAL anomaly has not changed significantly in the past 100 million years. These uncertainties indicate that we cannot use the isotopic data to quantitatively reconstruct Kohistan's paleolatitude in Cretaceous time; nevertheless it should be noted that the paleomagnetic study of Yoshida *et al.* (1996) place Kohistan slightly south of the Equator about 100 Ma ago.

Another way to look at these uncertainties is to try to minimize the size of the Shyok Sea. If we accept Searle's (1991) position for southern Asia at 10°N and a location for Kohistan closer to the northern limits of the DUPAL anomaly, perhaps along the equator, the Shyok Seaway shrinks in width to perhaps 1000 km. There is nothing in our data that precludes alternate configurations such as this.

## Conclusions

Geochemical and isotopic data reported here are most consistent with the model that the Kohistan intra-oceanic arc faced

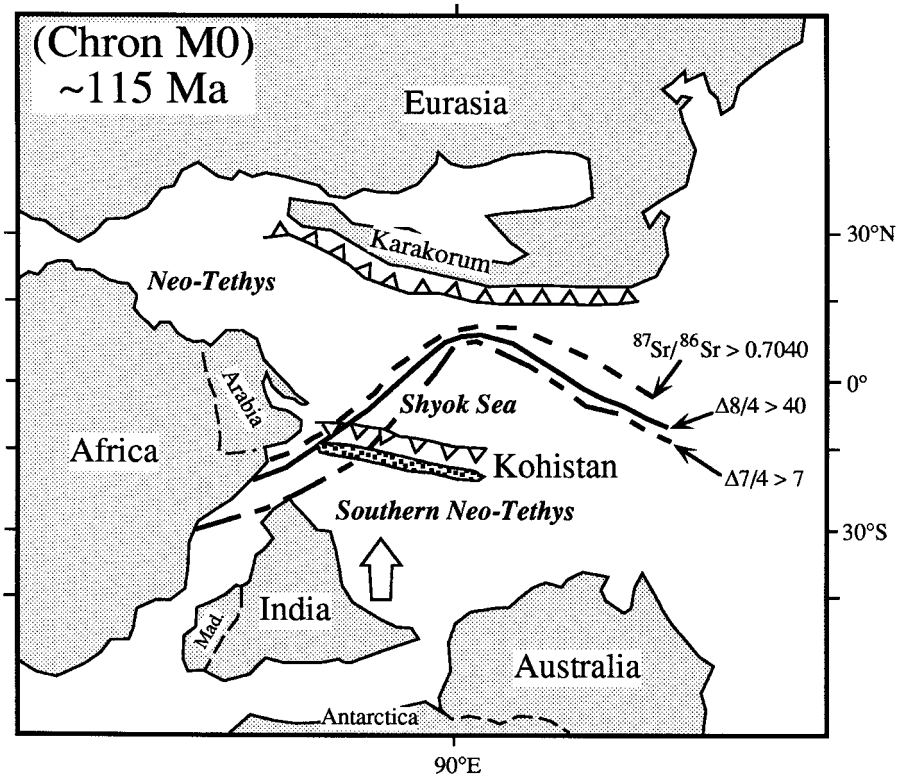


**Fig. 8.** Suggested palaeogeographic setting of the Kohistan arc during Aptian–Albian times. Positions of continents is generalized after Scotese *et al.* (1988, fig. 10), although the precise palaeolatitude of Asia is controversial. Present northern limits of DUPAL anomaly (located by $^{87}Sr/^{86}Sr > 0.7040$, $\Delta 7/4 > 7$ and $\Delta 8/4 > 40$) are from Hart (1984). Position of trenches and convergent plate margins are shown, with 'teeth' on the overriding plate. Note that during this time, Kohistan and India move northwards on the same plate. Compare this figure with Fig. 6a.

north, with forearc crust in the north (Chalt volcanics) and backarc crust in the south (Kamila amphibolites). The isotopic data indicate Kohistan igneous rocks formed by melting of a mantle source with a strong DUPAL isotopic signature. Such mantle sources exist in the oceanic realm far to the south of the present tectonic setting of Kohistan.

M.A.K. thanks the US Fullbright Program for support during 1993–1994. Isotopic studies at UTD were supported by NSF grant OCE-9302162. Field work was supported by NERC grant GR3/4242. M.A.K. acknowledges support for field work NSRDB project Esc. 24 and field assistance by M. Ahmed Khan and M. S. Qazi. B. L. Weaver arranged for XRF analyses at Norman. M. Q. Jan and B. L. Weaver provided Chilas analyses and samples for isotope analyses. We appreciate the thoughtful comments of S. Inger and P. Treloar. Thanks also to S. D. Kahn for reducing the data used to generate Fig. 5.

## Appendix: sample localities and descriptions

| | |
|---|---|
| A83 | Niat Gah, south of Lumar. Foliated, fine-grained metavolcanic amphibolite, otherwise homogeneous. |
| A86 | Niat Gah, north of Lumar. Fine-grained, metavolcanic amphibolite. |
| A93 | Niat Gah, 100 m north of the Niagran village (part of Niat metavolcanics). Dark, hornblende-rich metavolcanic amphibolite |
| A119 | Buto Gah, just north of village Sumal. Porphyritic meta-andesite, with relict pillow structure. |
| A121 | Buto Gah, 200 m south of village Chakhar. Meta-andesite, similar to A119. |
| A125 | Buto Gah, north of Chakkar. Niat-type metavolcanics |
| IK1007 | Eastern part of Thuly ultramafic body. Medium-grained noritic troctolite: PLAG–OPX–CPX–HB–SP. OL consumed in reaction to form OPX + HB |
| IK1009 | Thak bridge, Karakorum Highway. Peridotite dyke intruding the main ultramafic body. OL–HB–OPX–CPX–SP–CC–PLAG. |
| IK1012 | 10 m east of bridge near Chilas. Gabbronorite. Medium-grained, mildly foliated. PL–OPX–CPX–BIO–(opaque oxide–HB–KF–QZ–AP). |
| IK1017 | 17 km east of Sazin. Hypersthene quartz diorite. Medium-grained. PLAG–HB–OPX–CPX–QZ–KF–AP (titanite and zircon). |
| PL28 | About 3 km south of Chalt village, Hunza Valley; boninite. |
| PL29 | About 3 km south of Chalt village, Hunza Valley; andesite. |
| N115 | About 2 km south of Chalt village, Hunza Valley; rhyolite. |
| N116 | About 2 km south of Chalt village, Hunza Valley; basalt. |
| N138 | About 5 km south of Chalt village, Hunza Valley; calc-alkaline lava. |
| N139 | About 5 km south of Chalt village, Hunza Valley; rhyolite. |
| N161 | About 6.5 km south of Chalt village, Hunza Valley; boninite. |
| IK580 | 3 km south of Jaglot Gah, Hunza Valley; boninite. |

## References

BEARD, J.S. 1986. Characteristic mineralogy of arc-related cumulate gabbros: Implications for the tectonic setting. *Geology*, **14,** 848–851.

BLOOMER, S.H., TAYLOR, B., MACLEOD, C.J., STERN, R.J., FRYER, P., HAWKINS, J.W. & JOHNSON, L. 1995. Early Arc Volcanism and the Ophiolite Problem: A Perspective from Drilling in the Western Pacific. *In*: TAYLOR, B. & NATLAND, J. (eds) *Active Margins and Marginal Basins of the Western Pacific*. American Geophysical Union, Geophysical Monographs, **88,** 1–30.

COOPER, P.A. & TAYLOR, B. 1985. Polarity reversal in the Solomon Islands arc. *Nature*, **314,** 428–430.

COWARD, M.P., JAN, M.Q., REX, D., TARNEY, J., THIRLWALL, M. & WINDLEY, B.F. 1982. Structural evolution of a crustal section in the western Himalaya. *Nature*, **295,** 22–24.

——, WINDLEY, B.F., BROUGHTON, R.D., LUFF, I.W., PETTERSON, M.G., PUDSEY, C.J., REX, D.C. & KHAN, M.A. 1986. Collision tectonics in the NW Himalayas. *In*: COWARD, M.P. & RIES, A.C. (eds) *Collision Tectonics*. Geological Society, London, Special Publications, **19,** 203–219.

CRAWFORD, A.J., FALLOON, T.J. & GREEN, D.H. 1989. Classification, petrogenesis and tectonic setting of boninites. *In*: CRAWFORD, A.J. (ed.) *Boninites*. Unwin Hyman, London, 1–49.

DIETRICH, V.J., FRANK, W. & HONEGGAR, K. 1983. A Jurassic-Cretaceous island arc in the Ladakh Himalayas. *Journal of Volcanology and Geothermal Research*, **18,** 405–433.

FALLOON, T.J. & CRAWFORD, A.J. 1991. The petrogenesis of high-calcium boninite lavas dredged from the northern Tonga ridge. *Earth and Planetary Science Letters*, **102,** 375–394.

GRIBBLE, R.F., STERN, R.J., BLOOMER, S.H., STÜBEN, D., O'HEARN, T. & NEWMAN, S. 1996. MORB Mantle and Subduction Components Interact to Generate Basalts in the Southern Mariana Trough Back-Arc Basin. *Geochimica et Cosmochimica Acta*, **60,** 2153–2166.

HAMILTON, W.B. 1978. *Tectonics of the Indonesian Region*. US Geological Survey Professional Paper, **1078.**

—— 1994. Subduction systems and magmatism. *In*: SMELLIE, J.L. (ed.) *Volcanism Associated with Extension at Consuming Plate Margins*. Geological Society, London, Special Publications, **81,** 3–28.

HART, S.R. 1984. A large-scale isotope anomaly in the southern hemisphere mantle. *Nature*, **309,** 753–757.

—— 1988. Heterogeneous mantle domains: signatures, genesis and mixing chronologies. *Earth and Planetary Science Letters*, **90,** 273–296.

HARVEY, P.K. & ATKINS, B.P. 1982. The estimation of mass absorption coefficients by Compton scattering: Extensions to the use of Rh Kα Compton Radiation and intensity ratios. *American Mineralogist*, **67,** 534–537.

HAWKINS, J.W. 1995. Evolution of the Lau Basin—Insights from ODP Leg 135. *In*: TAYLOR, B. & NATLAND, J. (eds) *Active Margins and Marginal Basins of the Western Pacific*. American Geophysical Union, Geophysical Monographs, **88,** 125–173.

HONEGGER, K., DIETRICH, V., FRANK, W., GANSSER, A., THÖNI, M. & TROMMSDORFF, V. 1982. Magmatism and metamorphism in the Ladakh Himalayas (the Indus–Tsangpo suture zone). *Earth and Planetary Science Letters*, **60,** 253–292.

JAN, M.Q. 1988. Geochemistry of amphibolites from the southern part of Kohistan arc, N. Pakistan. *Mineralogical Magazine*, **52,** 147–159.

—— & HOWIE, R.A. 1980. Ortho- and clinopyroxenes from the pyroxene granulites of Swat Kohistan, northern Pakistan. *Mineralogical Magazine*, **43,** 715–726.

KHAN, M.A., JAN, M.Q. & WEAVER, B.L. 1993. Evolution of the lower arc crust in Kohistan, N. Pakistan: temporal arc magmatism through early, mature, and intra-arc rift stages. *In*: TRELOAR, P.J. & SEARLE, M.P. (eds) *Himalayan Tectonics*. Geological Society, London, Special Publications, **74,** 123–138.

——, ——, WINDLEY, B.F., TARNEY, J. & THIRLWALL, M.F. 1989. The Chilas mafic–ultramafic igneous complex: the root of the Kohistan island arc in the Himalaya of northern Pakistan. *In*: MALINCONICO, L.L. JR & LILLIE, R.J. (eds) *Tectonics of the Western Himalayas*. Geological Society of America, Special Papers, **232,** 75–94.

LEFORT, P., MICHARD, A., SONET, J. & ZIMMERMANN, J.L. 1983. Petrography, geochemistry, and geochronology of some samples from the Karakoram axial batholith (northern Pakistan). *In*: SHAMS, F.A. (ed.) *Granites of the Himalayas, Karakorum, and Hindu Kush*. Institute of Geology, Punjab University, Lahore, India, 377–387.

LEMAITRE, R.W. (ed.) 1989. *A Classification of Igneous Rocks and Glossary of Terms*. Blackwell, London.

LIGHTFOOT, P.C. & HAWKESWORTH, C.J. 1988. Origin of Deccan Trap lavas: evidence from combined trace element and Sr-, Nd- and Pb-isotope studies. *Earth and Planetary Science Letters*, **91,** 89–104.

——, ——, DEVEY, C.W., ROGERS, N.W. & VAN CALSTEREN, P.W.C. 1990. Source and Differentiation of Deccan Trap Lavas: Implications of Geochemical and Mineral Chemical Variations. *Journal of Petrology*, **32,** 1165–1200.

MANTON, W.I. 1988. Separation of Pb from young zircons by single-bead ion exchange. *Chemical Geology (Isotope Geoscience)*, **73,** 147–152.

MICHARD, A., BOUDIER, F. & GOFFÉ, B. 1991. Obduction versus Subduction and Collision in the Oman Case and Other Tethyan Settings. *In*: PETERS, TJ., NICOLAS, A. & COLEMAN, R.G. (eds) *Ophiolite Genesis and Evolution of the Oceanic Lithosphere*. Kluwer, London, 447–467.

MOORE, G.F., KADARISMAN, D., EVANS, C.A. & HAWKINS, J.W. 1981. Geology of the Talaud Islands, Molucca Sea collision zone, northeast Indonesia. *Journal of Structural Geology*, **3,** 467–475.

MORRIS, J., LEEMAN, W.P. & TERA, F. 1990. The subducted component in island arc lavas: constraints from Be isotopes and B-Be systematics. *Nature*, **344,** 31–36.

NESBITT, R.W., MASTINS, H., STOLZ, G.W. & BRUCE, D.R. 1976. Matrix corrections in trace element analysis by X-ray flourescence: an extension of the Compton scattering technique to long wavelengths. *Chemical Geology*, **18,** 203–213.

PATRIAT, P. & ACHACHE, J. 1984. India-Eurasia collision chronology has implications for crustal shortening and driving mechanism of plates. *Nature*, **311,** 615–621.

PEARCE, J.A. 1984. Role of sub-continental lithosphere in magma genesis at active continental margins. *In*: HAWKESWORTH, C.J. & NORRY, M.J. (eds) *Continental Basalts and Mantle Xenoliths*. Shiva, Nantwich, 230–249.

PEARCE, J.A., VAN DER LAAN, S.R., ARCULUS, R.J., MURTON, B.J., ISHII, T., PEATE, D.W. & PARKINSON, I.J. 1992. Boninite and harzburgite from Leg 125 (Bonin–Mariana forearc): A case study of magma genesis during the initial stages of subduction. *In*: FRYER, P., *ET AL.* (eds) *Proceedings of the ODP, Scientific Results*, **125.** Ocean Drilling Program, College Station TX, 623–662.

PENG, Z.X. & MAHONEY, J.J. 1995. Drillhole lavas from the northwestern Deccan Traps, and the evolution of Réunion hotspot mantle. *Earth and Planetary Science Letters*, **134,** 169–185.

PETTERSON, M.G. & WINDLEY, B.F. 1985. Rb-Sr dating of the Kohistan arc-batholith in the Trans-Himalaya of north Pakistan, and tectonic implications. *Earth and Planetary Science Letters*, **74,** 45–57.

—— & —— 1991. Changing source regions of magmas and crustal growth in the Trans-Himalayas: evidence from the Chalt volcanics and Kohistan batholith, Kohistan, northern Pakistan. *Earth and Planetary Science Letters*, **102,** 326–341.

——, CRAWFORD, M.B. & WINDLEY, B.F. 1993. Petrogenetic implications of neodymium isotope data from the Kohistan batholith, North Pakistan. *Journal of the Geological Society, London*, **150,** 125–129.

PIER, J.G., PODOSEK, F.A., LUHR, J.F., BRANNON, J.C. & ARANDA-GOMEZ, J.J. 1989. Spinel-lherzolite-bearing Quaternary volcanic centers in San Luis Potosi, Mexico. 2. Sr and Nd isotopic systematics. *Journal of Geophysical Research*, **94,** 7941–7951.

PUDSEY, C.J. 1986. The Northern Suture, Pakistan: margin of a Cretaceous island arc. *Geological Magazine*, **123,** 405–423.

RICHARD, P., SHIMIZU, N. & ALLÈGRE, C.J. 1976. $^{143}Nd/^{146}Nd$, a natural tracer. An Application to oceanic basalts. *Earth and Planetary Science Letters*, **31,** 269–278.

ROBERTSON, A. & DEGNAN, P. 1994. The Dras arc Complex: lithofacies and reconstruction of a Late Cretaceous oceanic volcanic arc in the Indus Suture Zone, Ladakh Himalayas. *Sedimentary Geology*, **92,** 117–145.

SCHÄRER, U., HAMET, J. & ALLÈGRE, C.J. 1984. The Transhimalya (Gangdese) plutonism in the Ladakh region: a U–Pb and Rb–Sr study. *Earth and Planetary Science Letters*, **67,** 327–339.

SCOTESE, C.R., GAHAGAN, L.M. & LARSON, R.L. 1988. Plate tectonic reconstructions of the Cretaceous and Cenozoic ocean basins. *Tectonophysics*, **155,** 27–48.

SEARLE, M.P. 1991. *Geology and Tectonics of the Karakoram Mountains*. John Wiley & Sons, Chichester.

STERN, R.J. & BLOOMER, S.H. 1992. Subduction zone infancy: Examples from the Eocene Izu-Bonin-Mariana and Jurassic California Arcs. *Geological Society of America Bulletin*, **104,** 1621–1636.

TAHIRKHELI, R.A.K., MATTAUER, M., PROUST, F. & TAPPONNIER, P. 1979. The India-Eurasia suture zone in Northern Pakistan: Synthesis and Interpretation of Recent Data at Plate Scale. *In*: FARAH, A. & DEJONG, K.A. (eds) *Geodynamics of Pakistan*. Geological Survey of Pakistan, Quetta, 125–130.

TAYLOR, R.N., MURTON, B.J. & NESBITT, R.W. 1992. Chemical transects across intra-oceanic arcs: implications for the tectonic setting of ophiolites. *In*: PARSON, L.M., MURTON, B.J. & BROWNING, P. (eds) *Ophiolites and their Modern Oceanic Analogues*. Geological Society of London Special Publications, **60,** 117–132.

TRELOAR, P., REX, D.C., GUISE, P.G., COWARD, M.P., PETTERSON, M.G., WINDLEY, B.F., LUFF, I.W. & JAN, M.Q. 1989. K/Ar and Ar/Ar geochronology of the Himalayas in N.W. Pakistan: Constraints on timing of collision, deformation, metamorphism and uplift. *Tectonics*, **8,** 881–909.

——, BRODIE, K.H., COWARD, M.P., JAN, M.Q., KHAN, M.A., KNIPE, R.J., REX, D.C. & WILLIAMS, M.P. 1990. The evolution of the Kamila shear zone, Kohistan, Pakistan. *In*: SALISBURY, M.H. & FOUNTAIN, D.M. (ed.) *Exposed Cross-Sections of the Continental Crust*. Kluwer Academic Press, Amsterdam, 175–214.

——, PETTERSON, M.G., JAN, M.Q. & SULLIVAN, M.A. 1996. A re-evaluation of the stratigraphy and evolution of the Kohistan arc sequence, Pakistan

Himalaya: Implications for magmatic and tectonic arc-building processes. *Journal of the Geological Society, London,* **153,** 681–693.

WOOD, D.A., MARSH, N.G., TARNEY, J., JORON, J.L., COTTEN, J. & TREUIL, M. 1981. Geochemistry of igneous rocks recovered from a transect across the Mariana Trough, Arc, Fore-arc, and Trench, Sites 453 through 461, Deep Sea Drilling Project Leg 60. *In*: HUSSONG, D.M. *ET AL.* (eds) *Initial Reports of the Deep Sea Drilling Project*, **60,** US Government Printing Office, Washington DC, 611–646.

YOSHIDA, M., ZAMAN, H. & AHMAD, M.N. 1996. Paleopositions of Kohistan Arc and surrounding terranes since Cretaceous Time: the Paleomagnetic Constraints. *Proceedings of Geoscience Colloquium, Geoscience Lab, Geological Survey of Pakistan*, **15,** 83–101.

ZARTMAN, R.E. & DOE, B.R. 1981. Plumbotectonics—the model. *Tectonophysics*, **75,** 135–162.

25 October 1996; revised typescript accepted 28 April 1997.
Scientific editing by Nick Rogers.